JOURNAL OF CATALYSIS 67, 348–361 (1981)

The Role of PtO_x in the Isothermal Rate Oscillations of Ethylene Oxidation on Platinum

C. G. VAYENAS, C. GEORGAKIS, J. MICHAELS, AND J. TORMO

Massachusetts Institute of Technology, Cambridge, Massachusetts 02139

Received May 23, 1980; revised September 3, 1980

A kinetic model has been developed to explain the oscillatory phenomena observed during the oxidation of ethylene on polycrystalline Pt films in a CSTR. Direct measurement of the oxygen activity on the Pt catalyst indicates that rate and oxygen activity oscillations are caused by the periodic formation and decomposition of surface platinum oxide. The model explains semiquantitatively all the experimental observations, i.e., that (1) oscillations occur on the fuel rich side only; (2) increasing rates correspond to decreasing surface oxygen activity; (3) there exist an upper and a lower temperature limit for oscillations; (4) the frequency of oscillations is a linear function of both the ethylene/O_2 ratio and the residence time in the CSTR. The thermodynamic properties of PtO_x are estimated from the oxygen activity measurements. The model may be applicable to other Pt-catalyzed oscillatory reactions as well.

INTRODUCTION

The oxidation of light hydrocarbon on Pt has attracted considerable attention in recent years due to the use of platinum as one of the active components in automotive exhaust catalytic converters. Work in this area prior to 1970 is summarized in several reviews (*1, 2*).

Ethylene oxidation on platinum has been the subject of several recent investigations. The metal has been dispersed on several supports such as silica (*3*) and Al_2O_3 (*4, 5*). In a more recent study a polycrystalline platinum film was used as the catalyst in a gradientless CSTR and the new technique of solid electrolyte potentiometry (SEP) (*6–8*) was applied to continuously monitor the activity of oxygen on the catalyst (*9*). It was found that over a well-defined temperature and gas-phase composition range both the rate of the reaction and the surface oxygen activity exhibit self-sustained isothermal oscillations. Several features of these oscillations were studied in detail including the simple dependence of limit cycle frequency on residence time and ethylene/O_2 ratio (*9*).

Periodic variations of conversion and temperature have also been observed during ethylene oxidation on supported platinum in a fixed-bed reactor (*5*). However, these oscillations were not isothermal and are certainly affected if not caused by heat and mass transfer limitations in the catalytic bed.

Rate oscillations during isothermal or nearly isothermal catalytic oxidation of CO and hydrogen have been observed over various forms of platinum catalysts as well as during H_2 oxidation on Pd and Ni (*10–12, 15–21*). Oscillations in the EMF of solid-state oxygen concentration cells used in nonequilibrium CO, O_2 environments have been also reported and attributed to periodic catalytic phenomena on the platinum electrode (*22*). Trace hydrocarbon impurities have a pronounced effect on the periodic behavior of the oxidation of CO on Pt (*23*).

Several kinetic mechanisms have been proposed to explain the oscillatory behavior of these catalytic oxidations. They are based on one of the following assumptions (*18*): (a) strong dependence of the activation energy or heat of adsorption on surface coverage (*10, 12, 13, 21*), (b) periodic oxidation and reduction of the surface (*11, 12, 15*), (c) shift between multiple steady states due to slow adsorption or

0021-9517/81/020348-14$02.00/0

desorption of an inert species (*14*), and (d) surface temperature oscillations (*20*).

Mathematical models based on these assumptions have, in the best cases, given only rough qualitative agreement with experiment (*12*). Clearly some knowledge of surface concentrations of adsorbed species is necessary in order to better understand the oscillatory phenomena and discriminate among various models. Such a discrimination could be also greatly facilitated by systematic experimental study of the characteristic features of the oscillations, e.g., frequency dependence on temperature and gas phase composition, as was done during ethylene oxidation on platinum.

In the present communication a model is presented which explains the ethylene oxidation oscillations in a more natural way. The model is based on the information provided by the electrochemical oxygen activity measurement (SEP). This simple new technique, in which the catalyst film under study also serves as one of the electrodes of a solid electrolyte oxygen concentration cell, was originally proposed by Wagner (*6*) and has been used recently to study the mechanism of several catalytic oxidations (*7–9*). The technique has been described in detail elsewhere (*6, 9*). It will be shown that the surface oxygen activity measurements strongly support a surface oxidation–reduction mechanism in which oscillations result from periodic formation and destruction of surface platinum oxide.

That surface platinum oxides exist and can act as a means of storing oxygen on Pt surfaces has been shown conclusively by the work of Ostermaier *et al.* (*24*). Oxide formation introduces a variability into the surface properties of platinum, that makes the catalyst respond slowly to changes in gas-phase compositions (*3, 26*). Recent UHV studies on the interaction of oxygen with Pt (*25, 26*) have shown the existence of several types of chemisorbed oxygen: molecularly chemisorbed oxygen, which is present in measurable coverages only below 200 K but acts as a precursor state for atomic chemisorption at higher temperatures, and two types of dissociatively chemisorbed oxygen one of which forms the well-known ordered (2 × 2) LEED pattern and platinum oxide (*25*). All these recent studies show that in oxidation reactions platinum may not be as noble a metal as usually assumed.

EXPERIMENTAL METHODS

The experimental apparatus and the platinum catalyst preparation and characterization procedure is described in detail elsewhere (*9, 27*). Englehard A-3788 Pt paste was used to deposit the Pt film catalyst electrode which was dried and calcined in air at 600°C for 5 h. The catalyst was used without any further pretreatment. The porous catalyst film had a superficial surface area of 2 cm^2 and could adsorb approximately $(8 \pm 2) \cdot 10^{-7}$ moles O_2 as determined by oxygen chemisorption followed by titration with ethylene (*9*).

The reactor volume was 30 cm^3 and over the range of flow rates used (150–700 cm^3 STP/min) behaves as a well-mixed reactor as shown in Fig. 1. Reactants were Matheson Certified Standard C_2H_4 diluted in N_2 and Matheson zero gas air. They could be further diluted with N_2. Replacing zero gas air with commercial compressed air was found to have no effect on the oscillations. The open-circuit emf E of the oxygen concentration cell, was mesured by means of a differential voltmeter (J. Fluke 891A) with an input resistance of 10^8 Ω and infinite resistance at nul. The emf E is related to the oxygen activity a_O by means of the Nernst equation (*9*)

$$E = \frac{RT}{4F'} \ln \frac{a_O^2}{(0.21)}, \qquad (1)$$

where F' is the Faraday constant and (0.21) is the activity of oxygen on the reference Pt electrode which is in equilibrium with air, the reference gas. Further experimental details are given in Refs. (*9, 27*).

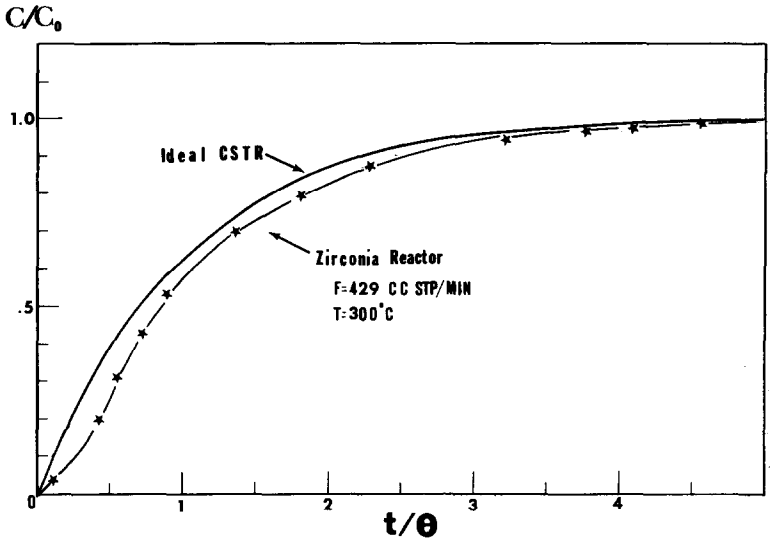

FIG. 1. Reactor response to a step change in inlet CO_2 concentration. Mean residence time $\theta = 2.18$ s. Detector: ir CO_2 analyzer.

RESULTS

Summary of Experimental Results

The reaction kinetics were studied at temperatures between 200 and 400°C, ethylene partial pressures up to 0.02 bar, and oxygen partial pressures up to 0.2 bar. The inlet stream impinged directly on the catalyst film with velocities of the order of 1–2 m/s, and the rate was shown to be totally unaffected by diffusional limitation (*9, 27*). The oscillations are isothermal at least within 0.5°C as was determined by attaching a small thermocouple directly to the catalyst film and observing no temperature oscillations and less than 2°C difference between the catalyst film and the ambient gas temperature.

The steady state and the oscillatory behavior of the system have been described in detail elsewhere (*9*), and are summarized in paragraphs a–d and f–h below. In paragraph e we also add a few more recent findings.

a. Over the range of conditions investigated the oxygen activity on platinum a_O[2] drops well below the gas-phase activity value P_{O_2}. This is true both during steady state and during oscillations. At steady state it satisfies the equation

$$a_O = K_S P_{O_2}/P_{ET}, \tag{2}$$

where

$$\ln K_S = 7.7\ (\pm 2.0) - 18{,}000\ (\pm 2000)/RT. \tag{3}$$

The magnitude of K_S is found to differ by as much as a factor of 2 for different catalyst films probably due to crystallite size effects. Equation (2) was also approximately valid during oscillations since the amplitude of the emf oscillations was small, typically less than 5% of the absolute emf value.

b. The steady-state kinetics on both the fuel-rich and fuel-lean sides can be described fairly well by the rate expression

$$r = K_1 K_2 P_{ET} P_{O_2}/(K_1 P_{O_2} + K_2 P_{ET}), \tag{4}$$

where

$$K_1 = 140 \exp(-16{,}700/RT) \text{ mole/s}, \tag{5}$$

$$K_2 = 5.8 \cdot 10^{-3} \exp(-5000/RT) \text{ mole/s}. \tag{6}$$

The apparent activation energy is high (~17 kcal/mole) on the fuel-lean side and low (~5 kcal/mole) on the fuel-rich side.

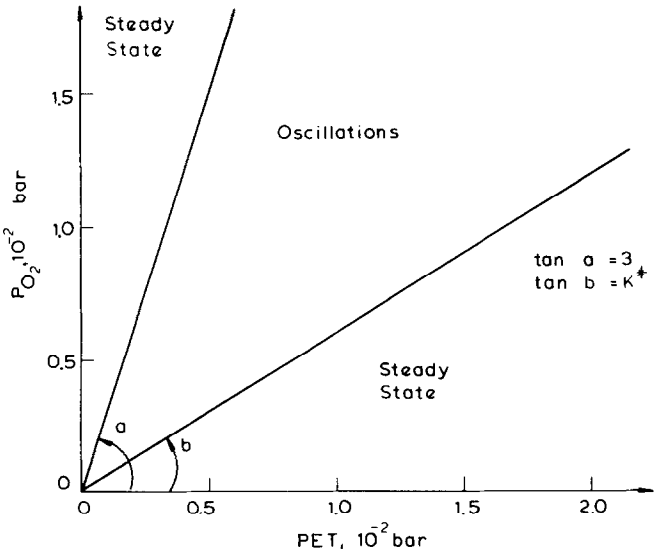

FIG. 2. Oxygen–ethylene concentration plane illustrating the region where all oscillatory states are observed at 300°C. The value of K^* varies with temperature according to Fig. 4 and Eq. (32).

Since the amplitude of rate oscillations is typically less than 10% of the rate, Eq. (4) can be used to estimate the average rate of CO_2 formation in the oscillatory region as well.

c. Rate and surface oxygen activity oscillations occur on the fuel-rich side only (Fig. 2).

d. During an oscillation increasing rate always corresponds to decreasing a_O.

e. Oscillations take place only over a narrow and well-defined range of a_O values (9). The upper limit is equal to $3K_s$, where K_s is defined by Eq. (3). This upper limit simply reflects the fact that oscillations occur on the fuel-rich side only. As this limit is approached the frequency of oscillations becomes zero. At the lower limit a_O^* the frequency approaches infinity. When $a_O < a_O^*$ a stable steady state is obtained. The temperature dependence of a_O^* (sharp transition between oscillatory and nonoscillatory states) is shown in Fig. 3. It corresponds to

$$a_O^* = 2.7 \cdot 10^5 \exp(-23{,}900/RT)\text{bar}^{1/2}. \quad (7)$$

There is no obvious physical meaning of a_O^*. We will postulate that it corresponds to the thermodynamic stability limit of surface platinum oxide. This is the only major

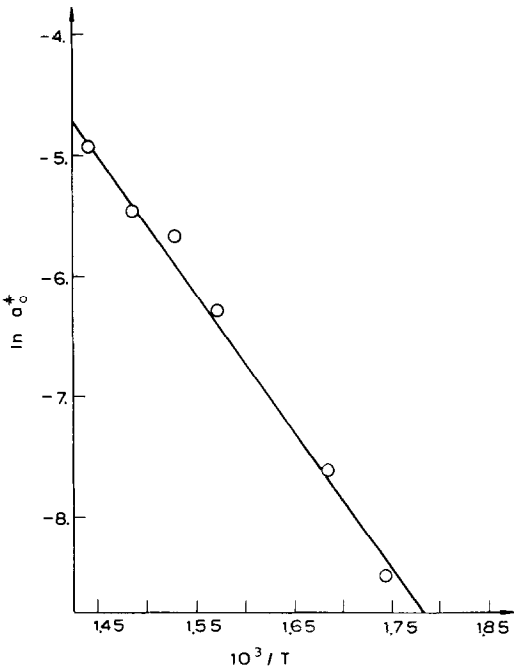

FIG. 3. Temperature dependence of a_O^*. Oscillations occur with $a_O > a_O^*$.

assumption of the model and is justified below. In light of (2) the equality $a_O = a_O^*$ defines a second straight line on the oxygen–ethylene concentration plane which corresponds to $P_{O_2}/P_{ET} = a_O^*/K_s K^*(T)$ and separates oscillatory and nonoscillatory states. This is shown in Fig. 2. The experimentally observed temperature dependence of K^* is shown in Fig. 4.

f. At constant flow rate and constant fuel-rich inlet gas composition there exist a lower and an upper temperature limit for oscillations. As shown under Discussion, this is a direct consequence of e. Although these two temperature limits depend on space velocity and inlet ethylene/O_2 ratio N_3, typical values are 260 and 360°C for the lower and upper limits, respectively (*9*).

g. At constant temperature and residence time the frequency of the limit cycles ν is proportional to N_3-γ, where N_3 is the inlet ethylene/O_2 ratio and γ is a constant. The value of γ is 0.6 at T = 300°C (Fig. 7a).

h. At constant temperature and N_3 the frequency of oscillations ν is an increasing function of the residence time θ. The dependence is almost linear (Fig. 8a).

The mathematical model proposed in the following section will be shown to predict all of the above experimental observations.

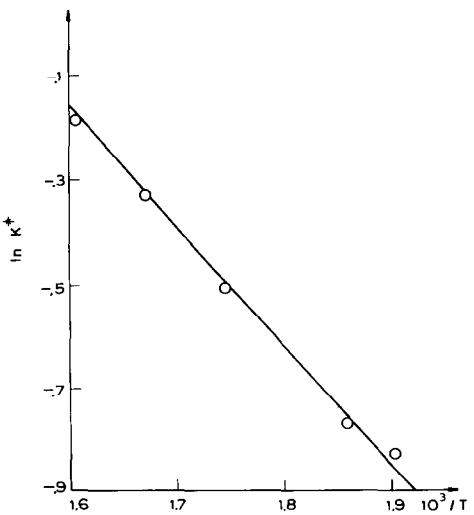

FIG. 4. Temperature dependence of K^*. Oscillations occur with $P_{O_2}/P_{ET} > K^*$.

Development of the Mathematical Model

We start the development of the mathematical model by postulating a mechanism for the reaction. The mechanism is a logical extension of that proposed in (*9*) which accounts for the steady-state ethylene oxidation kinetics on platinum. As will be shown in later sections this extended mechanism is able to reproduce semiquantitatively all the observed experimental data. Before settling on the proposed mechanism, others were examined and rejected because they could not reproduce the experimental results in a satisfactory way, as is briefly discussed at the end of this section.

In agreement with previous experimental UHV studies of the interaction of oxygen with Pt (*24–26*) we postulate the existence of two types of Pt adsorption sites for atomic oxygen. The first type of site, denoted by m, with a total concentration of C_m produces reactive dissociatively chemisorbed oxygen. The other type of site, denoted by l, with a total concentration of C_l are those that produce surface platinum oxide PtO_x. To the extent that PtO_x is thermodynamically stable, i.e., the ambient oxygen activity is higher than that defined by the oxide stability limit (Eq. (7)), the oxide is assumed to be unreactive with ethylene. This surface platinum oxide may not necessarily be the oxide reported in (*24*). It could correspond to the second type of atomically chemisorbed oxygen, the "ordered oxygen structure," reported in (*25*) or the unreactive second type of chemisorbed oxygen found on polycrystalline platinum in (*26*). By denoting with m · O the atomically chemisorbed reactive oxygen and by l · O the oxygen present in the Pt oxide form the proposed mechanism can be written as follows

$$\frac{1}{2}\left\{\begin{array}{ll} O_2(g) + m \xrightarrow{K_1} m \cdot O_2 & (8a) \\ m \cdot O_2 + m \rightleftarrows 2m \cdot O & (8b) \end{array}\right\},$$

$$C_2H_4(g) + m \cdot O \xrightarrow{K_2}$$

$$P \xrightarrow[+\frac{3}{2}O_2(g)]{FAST} 2CO_2 + 2H_2O + m, \quad (9)$$

$$m \cdot O + 1 \xrightarrow{K_3} m + 1 \cdot O, \quad (10)$$

$$C_2H_4(g) + 6\,1 \cdot O \xrightarrow{K_4}$$

$$6\,1 + 2CO_2 + 2H_2O, \quad (11)$$

where P is a highly reactive intermediate.

Steps (8a), (8b), and (9) have been shown in (*9*) to describe accurately the steady-state kinetics and surface oxygen activity behavior. This is also shown below. Steps (10) and (11) have been added in order to account for the oscillations.

Steps (8a) and (8b) represent the chemisorption of atomic oxygen via a molecularly absorbed precursor state. Step (8b) is assumed to be always in equilibrium so that (8a) is rate limiting for oxygen chemisorption. It was shown in (*9*) that with these assumptions the rate of atomic oxygen chemisorption can be expressed as

$$r_i = K_1 P_{O_2}(1 - \theta_1), \quad (12)$$

where θ_1 is the fraction of "m"-type sites covered with O · m. The third reaction (9) involves the existence of an intermediate complex P which is rapidly oxidized to the combustion products. The reaction rate is taken as

$$r_2 = K_2 P_{ET} \theta_1. \quad (13)$$

By denoting with θ_2 the fraction of oxide sites "1" covered with oxygen the rate of reaction (*3*) is written as

$$r_3 = K_3 \theta_1 (1 - \theta_2). \quad (14)$$

This reaction takes place only when the oxide form is stable. When the conditions change so that a preexisting amount of PtO_x becomes unstable, reaction (11) is assumed to take place with a rate

$$r_4 = K_4 P_{ET} \theta_2. \quad (15)$$

The platinum oxide is taken as stable when P_{O_2}/P_{ET} is greater than a constant $K^*(T)$ given by

$$K^*(T) = a_O^*(T)/K_s(T). \quad (16)$$

This critical parameter corresponds to the sharp transition between oscillatory and nonoscillatory states and has been accurately determined over the temperature range of interest (Fig. 4). In light of Eqs. (2) and (16) the inequality $P_{O_2}/P_{ET} > K^*(T)$ is equivalent to $a_O > a_O^*(T)$ at steady state. However, during transients, Eq. (2) is only approximately satisfied and thus the two oxide stability criteria $P_{O_2}/P_{ET} > K^*(T)$ and $a_O > a_O^*(T)$ are not physically or mathematically equivalent. The former would correspond to rapid equilibration of Pt oxide with the gas phase, probably through a second precursor state associated with 1 sites; the latter would imply a rapid equilibration between oxide and chemisorbed oxygen, the activity of which (a_O) is being monitored. We have chosen the former criterion on the following grounds:

a. It is rather well established (*25*) that the production of surface oxide can proceed through a molecular precursor state which is in equilibrium with the gas phase. It is reasonable to assume that during transients this second precursor state remains in equilibrium with the gas phase but not necessarily with chemisorbed oxygen.

b. If the latter criterion is used the model cannot explain the experimentally observed decrease in a_O with increasing rate. Futhermore the model does not predict oscillations.

By use of the mechanism postulated above and the assumed reaction rates, the transient mole balances for oxygen and ethylene in the gaseous phase are

$$V \frac{dc_1}{dt_*} = F(c_{1f} - c_1) - \frac{1}{2} Sk_1 \frac{c_1}{c_T}(1 - \theta_1) - \frac{5}{2} Sk_2 \frac{c_2}{c_T} \theta_1, \quad (17)$$

$$V \frac{dc_2}{dt_*} = F(c_{2f} - c_2) - Sk_2 \frac{c_2}{c_T} \theta_1 - \alpha SK_4 \frac{c_2}{c_T} \theta_2. \quad (18)$$

Here α is a Heaviside function

$$\alpha = H\left(K^* - \frac{P_{O_2}}{P_{ET}}\right) = H\left(K^* - \frac{c_1}{c_2}\right) = \begin{cases} 0 \text{ if } \frac{c_1}{c_2} > K^* \\ 1 \text{ if } \frac{c_1}{c_2} < K^*. \end{cases} \quad (19)$$

On the other hand a balance for the "m" and "l" sites yields

$$SC_m \frac{d\theta_1}{dt*} = Sk_1 \frac{c_1}{c_T}(1 - \theta_1) - Sk_2 \frac{c_2}{c_T}\theta_1 - (1 - \alpha)Sk_3\theta_1(1 - \theta_2), \quad (20)$$

$$SC_l \frac{d\theta_2}{dt*} = (1 - \alpha)Sk_3\theta_1(1 - \theta_2) - 6\alpha Sk_4 \frac{c_2}{c_T}\theta_2. \quad (21)$$

To nondimensionalize the model we normalize the gaseous concentrations with respect to the inlet oxygen concentration and time with respect to the space time of the reactor, V/F. It then follows that

$$\frac{dx_1}{dt} = 1 - x_1 - \frac{1}{2}N_1x_1(1 - \theta_1) - \frac{5}{2}N_2x_1, \quad (22)$$

$$\frac{dx_2}{dt} = N_3 - x_2 - N_2x_2\theta_1 - \alpha N_2x_2\theta_2, \quad (23)$$

$$N_5 \frac{d\theta_1}{dt} = N_1x_1(1 - \theta_1) - N_2x_2\theta_1 - (1 - \alpha)N_7\theta_1(1 - \theta_2), \quad (24)$$

$$N_6 \frac{d\theta_2}{dt} = (1 - \alpha)N_7\theta_1(1 - \theta_1) - 6\alpha N_4x_2\theta_2, \quad (25)$$

where N_1–N_7 are dimensionless numbers defined in nomenclature. The numbers N_1, N_2, N_4, and N_7 are ratios of the reactor residence time over the corresponding reaction time for reactions (8), (9), (11), and (10), while N_3 is the ratio of ethylene to oxygen inlet concentrations or partial pressures. $N_3 = \frac{1}{3}$ corresponds to a stoichiometric feed composition, and fuel-rich conditions correspond to values of N_3 greater than $\frac{1}{3}$. The dimensionless numbers N_5 and N_6 represent ratios of the maximum amounts of chemisorbed oxygen, and oxide oxygen, respectively, to the amount of gas-phase oxygen in the reactor.

At steady state the time derivatives are equal to zero, and for the case of $\alpha = 0$ one obtains $\theta_{2s} = 1$ and

$$\theta_{1s} = N_1x_{1s}/(N_1x_{1s} + N_2x_{2s}). \quad (26)$$

The last equation can be rewritten as

$$\frac{\theta_{1s}}{1 - \theta_{1s}} = \frac{N_1x_{1s}}{N_2x_{2s}}, \quad (27)$$

which reduces to the experimental steady-state equation (2) if one assumes a Langmuir isotherm for oxygen chemisorption on m sites. This assumption has been shown in (9) to be consistent with steps (8a) and (8b), which describe oxygen chemisorption on m sites. It also follows from (26) that the rate of ethylene oxidation is

$$R_s = N_2x_{2s}\theta_{1s} = \frac{N_1N_2x_{1s}x_{2s}}{N_1x_{1s} + N_2x_{2s}}, \quad (28)$$

which is dimensionless form of Eq. (4). The values of x_{1s} and x_{2s} can then be found from the equations

$$0 = 1 - x_{1s} - 3\frac{N_1N_2x_{1s}x_{2s}}{N_1x_{1s} + N_2x_{2s}}, \quad (29)$$

$$0 = N_3 - x_{2s} - \frac{N_1N_2s_{1s}x_{2s}}{N_1x_{1s} + N_2x_{2s}}. \quad (30)$$

Consequently the steady state lies on the line

$$x_{2s} = N_3 - \tfrac{1}{3}(1 - x_{1s}) \quad (31)$$

in the (x_1, x_2) plane.

On the other hand if $\alpha = 1$ the steady state corresponds to $\theta_{2s} = 0$. However, Eqs. (26–31) still remain valid.

It can be easily shown that the mechanism presented in (9) always predicts a stable steady state in a CSTR. It never produces oscillations. We found that limit cycles can be predicted by a second mechanism which accounts for the existence of

surface oxide and assumes that when the oxide becomes thermodynamically unstable, oxygen associated with the oxide is converted into chemisorbed oxygen m · O, instead of reacting with ethylene according to (11). However, this second model was discarded because it fails to predict the observed decrease in surface oxygen activity with increasing rate during oscillations.

Dimensionless Parameter Evaluation and Estimation

The dimensionless groups N_1, N_2 are on the order of 0.1–1 and calculated at any temperature and flowrate using Eqs. (5, 6) that describe the temperature dependence of $Sk_1 = K_1$, and $Sk_2 = K_2$. The group N_3 can be directly obtained from the inlet conditions. To calculate N_5 and N_6 the parameters $C_m \cdot S$ and $C_1 \cdot S$ must be known. The reactive oxygen uptake of the Pt catalyst used has been independently measured (*9*) and found to be 8 $(\pm 2) \cdot 10^{-7}$ mole O_2. This must correspond to $C_m \cdot S + C_1 \cdot S$. Because of the lack of any further information we will assume $C_m = C_1$. This approximation leads to reasonably good agreement between the model predicted and the experimentally observed (a) amplitude of rate oscillations, which is proportional to $C_1 \cdot S$ and (b) amplitude of emf oscillations, which depends heavily on $C_m \cdot S$. Consequently N_5 and N_6 are of the order of 0.1–0.2. The parameters N_4 and N_7 depend on the rate constants k_3 and k_4 of the fast reactions (*10, 11*) that could not be measured independently. However, the model predictions are quite insensitive to the numerical values of N_4 and N_7 provided $N_4 \gg N_1$, N_2, and $N_7 > N_1$, N_2.

A key parameter of the model is $K^*(T)$, defined as the critical oxygen-to-ethylene ratio $(P_{O_2}/P_{ET})^*$, which corresponds to the oxide stability limit. This parameter is obtained directly from Fig. 4, and can be expressed by

$$K^*(T) = 20.1 \exp(-4000/RT). \quad (32)$$

It should be noted that according to Eq. (2) the experimental parameter K_s should also satisfy Eq. (16). Substituting $K^*(T)$ from (32) and a_0^* from (7) into (16) one obtains $K_s = 1.3 \cdot 10^4 \cdot \exp(-19{,}900/RT)$, which is within the experimental error of K_s obtained from steady-state data (Eq. (3)). This illustrates the internal consistency of the experimental values of parameters used in the model.

Finally to calculate the emf, E from θ_1, one must use Eq. (1) together with the Langmuir isotherm for oxygen chemisorbed on m type sites which follows from Eqs. (27) and (2) and is valid for any gas-phase composition (*9*):

$$K_O a_O = \theta_1/(1 - \theta_1). \quad (33)$$

According to Eqs. (33), (27), and (2), K_O equals K_1/K_2K_s and thus can be calculated directly at any temperature from (3), (5), and (6). Thus the emf E can be calculated from (1) and (33) at any temperature and oxygen coverage θ_1. Equation (33) is valid provided ethylene does not chemisorb on m sites. It should be noted that the proposed model does not exclude the possibility of ethylene adsorption on other types of sites provided the ethylene coverage is low and proportional to P_{ET}. The low ethylene coverage assumption is not unreasonable in view of the relatively high temperatures employed in the kinetic study.

Model Predictions and Comparisons with Experiment

The system of equations (22–25) was solved numerically using the Euler integration method which was easier to apply than the Runge–Kutta method because of the discontinuity in θ_2 at the oxide stability limit. Model-predicted oscillations of P_{CO_2}, emf E, P_{O_2}, and oxide coverage θ_2 are shown in Fig. 6 for typical operating conditions. The experimentally observed oscillations under the same conditions are shown in Fig. 5. There is very good agreement between experimental and model-pre-

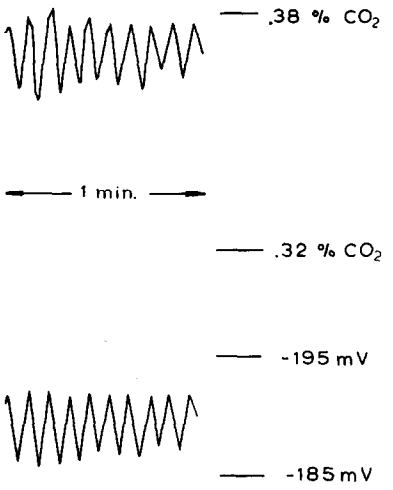

FIG. 5. Experimentally observed oscillations: Feed composition: $P_{ET}^0 = 1.74 \cdot 10^{-1}$ bar, $P_{O_2}^0 = 1.6 \cdot 10^{-2}$ bar, $T = 573$ K, flow rate 218 cm³ STP/min. Frequency of oscillations: 0.24 s^{-1}.

dicted frequencies of oscillations. The predicted amplitude of exit CO_2 concentration oscillation is also in good agreement with experiment. The model predicts emf oscillation amplitudes considerably higher than the experimental value.

The model frequently fails to predict oscillations under conditions where they have been observed, especially for N_3 values below 1. This is shown in Figs. 7b and 8b. However, when the model predicts oscillations, agreement with experiment is always good, especially regarding the frequency and amplitude of the CO_2 concentration oscillation.

The model predicts fairly well the experimentally observed quasi-linear increase of limit cycle frequency with increasing feed ethylene/oxygen ratio N_3 (Fig. 7).

It also predicts nicely the almost linear increase in limit cycle frequency with increasing residence time (Fig. 8).

The experimentally observed existence of upper and lower temperature limits for oscillations at constant N_3 and θ, which is described in detail in (9), is also explained by the model as shown in Fig. 9. At the low

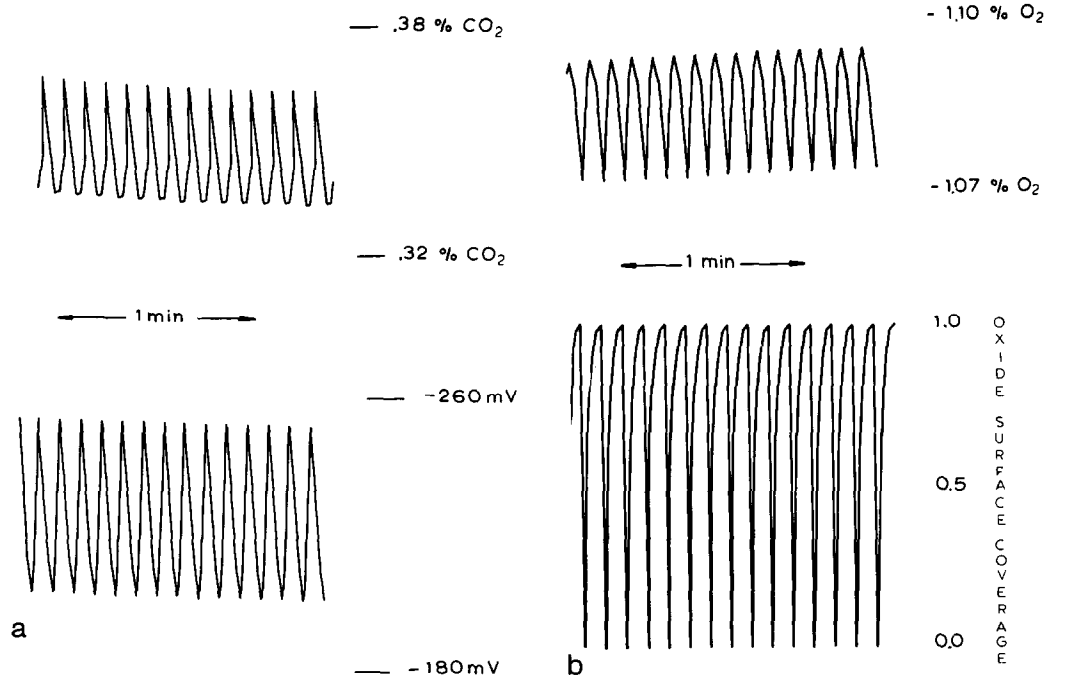

FIG. 6. Model predicted oscillations under the same conditions as in Fig. 5 (a) P_{CO_2} and emf (b) P_{O_2} and θ_2. Frequency of oscillations = 0.26 s^{-1}.

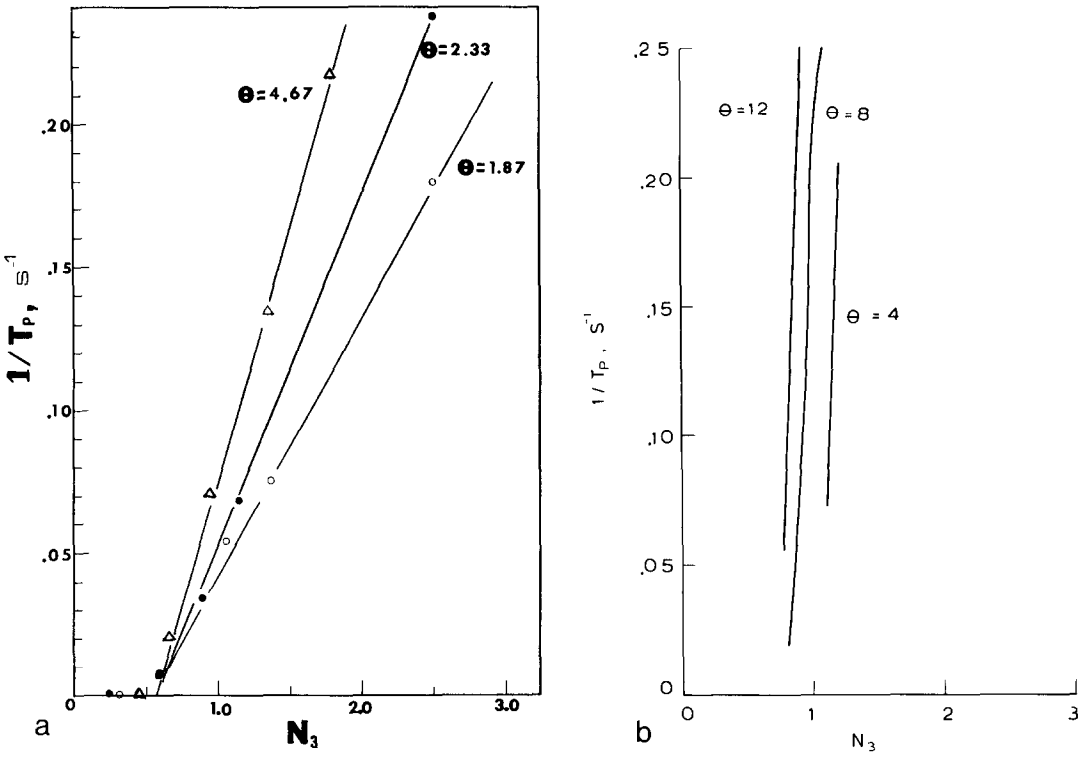

FIG. 7. Limit cycle frequency dependence on inlet ethylene/oxygen ratio N_3. (a) Experimental; (b) model prediction, T = 300°C.

temperature, conversion is low, the oxide is stable, and the system reaches a stable steady state. At intermediate temperatures conversion increases and the oxide stability line moves up; thus the system is caught in a limit cycle. At higher temperatures the system reaches a steady state, since it never crosses the oxide stability line.

The numerical solution was usually initialized with the reactor inlet conditions. At constant temperature, flow rate, and inlet composition the model-predicted limit cycle was shown to be independent of the initial state of the system as long as the initial composition is on the same side of the oxide stability limit as the feed composition.

DISCUSSION

The proposed model describes in a satisfactory way the experimentally observed oscillatory behavior of ethylene oxidation on polycrystalline Pt. Within a factor of 2 it gives the right frequencies and P_{CO_2} oscillation amplitudes and also predicts all the important features of the oscillations outlined under Experimental Results. It also accurately predicts the steady-state behavior of the system.

A physical interpretation of model predictions and comparison with experiment is given below. Figure 10 shows schematically the stoichiometric line OS and the oxide stability limit OT on a dimensionless oxygen–ethylene concentration plane at 300°C. The slope of OT is 0.6 according to Fig. 2. The inlet composition may correspond to any point P on line MZ. Because of the reaction stoichiometry (Eq. (31)) the locus of all possible states in the CSTR is a straight line of slope 3 passing from P.

It becomes clear that if P is between points M and S, e.g., at P_1, then the locus of

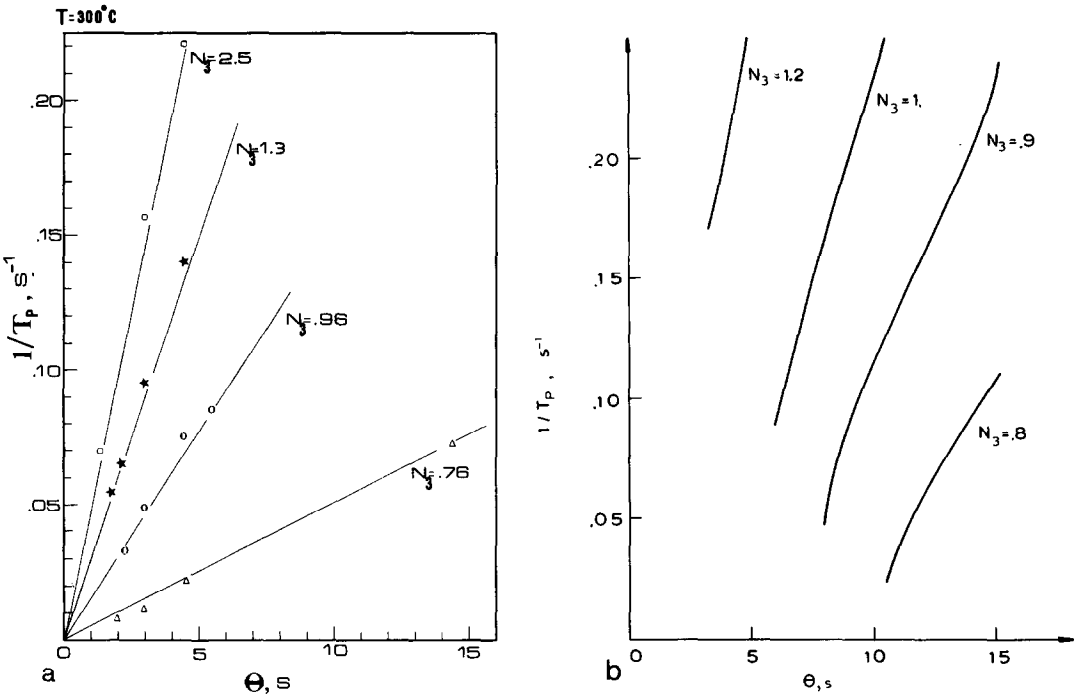

FIG. 8. Limit cycle frequency dependence on residence time θ, (a) Experimental; (b) model prediction, T = 300°C.

steady states P_1P_1' never intersects the oxide stability limit, i.e., oscillations can never take place on the fuel-lean side for this reaction, in excellent agreement with experiment. Interestingly enough if the stoichiometric fuel/O_2 ratio of the reaction were smaller than 1 (e.g., CO oxidation) then the model would predict oscillations on the fuel-lean side, which is exactly what has been observed with CO oxidation (*22*). This is, however, simply speculation as it is not known if an equation similar to (2) is valid during CO oxidation.

If on the other hand the inlet composition corresponds to P_4, i.e., $(P_{O_2}/P_{ET}) < K^*$, then again no oscillations can take place since the system can reach any steady state on P_4P_4' without ever crossing the oxide stability limit OT, again in excellent agreement with experiment. If, however, the inlet composition lies between points S and T, e.g., P_2, then it is possible to observe limit cycles. Such a limit cycle is shown in Fig. 10. If the steady state S_2 is between points A and P_2' then the system hits the oxide stability limit on its approach to steady state at point A. At this point the oxide becomes unstable, reacts with ethylene according to (11) thus causing a rapid decrease in ethylene concentration AA_1 and a spike in P_{CO_2} which is observed experimentally. At this point A_1 oxide formation is thermodynamically favored and takes place (10) until the system again hits the oxide stability limit on its approach A_1A_3 to S_2. The system is thus caught in a limit cycle A_2A_3.

The period of the limit cycle is determined by the time required for the system to travel from A_2 to A_3 as it is assumed to go from A_3 to A_2 essentially instantaneously ($N_4 \gg N_1, N_2$). Because the net change in gas-phase ethylene concentration is small, this time is inversely proportional to the average value of the dimensionless rate in the vicinity of point A. Comparing therefore the limit cycle frequencies ν_A and ν_B at points A and B we conclude that their ratio

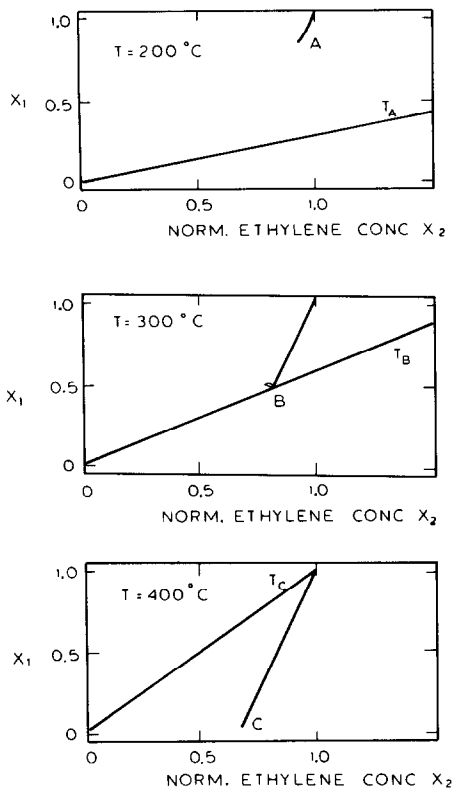

FIG. 9. Temperature effect on oscillations at constant N_3 = 1 and flow rate F = 100 cm³ STP/min. States A and C are stable. State B is an oscillatory state. x_1 = normalized oxygen concentration. Experimental upper and lower limits for oscillations (9) = 360–240°C.

must equal the ratio of the average steady-state rates at points A and B.

$$\nu_A/\nu_B = r_A/r_B. \tag{34}$$

According to Eq. (28) this ratio must also equal $x_{2,A}/x_{2,B}$ since the ratio x_1/x_2 is constant along the line OT. It thus follows that $\nu_A/\nu_B = x_{2,A}/x_{2,B}$ and from the similar triangles $OX_{2A}A$ and $OX_{2B}B$ one obtains $\nu_A/\nu_B = (OA)/(OB)$; therefore $\nu_A/\nu_B = (P_2S)/(P_3S)$. This explains why the frequency is found to be a linear function of N_3 both according to the model and according to experiment (Fig. 7).

The model relies heavily on the assumption that a_0^* is indeed the stability limit of surface platinum oxide. This is certainly justified by the impressive agreement between model predictions and experiment. Also the ΔH and ΔS values obtained from the temperature dependence of a_0^* (Eq. (7)) are very reasonable. The ΔH value of −46 kcal/mole O_2 is in good agreement with the heat of atomic chemisorption of O_2 on Pt recently reported by Gland and Korchak (25). The ΔS value of −45 e.u. is in very good agreement with the expected value for a reaction of the form

$$2\text{Pt(s)} + \text{O}_2\text{(g)} \rightleftarrows 2\text{PtO(s)}.$$

Supported small-size Pt crystallites are known to become oxidized much more

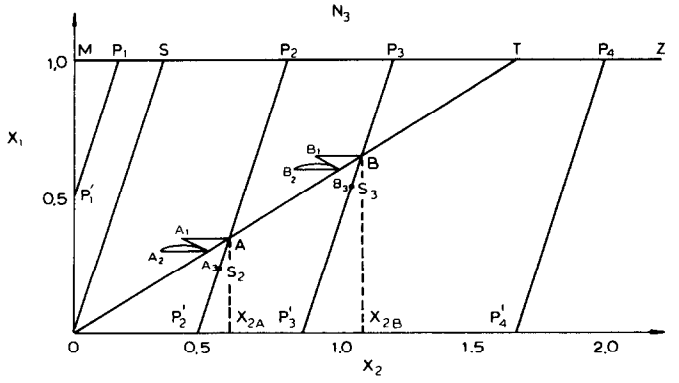

FIG. 10. Dimensionless oxygen (x_1), ethylene (x_2) concentration plane illustrating the effect of inlet ethylene/oxygen ratio N_3 on the reactor behavior. Symbols defined under Discussion. Temperature = 300°C.

readily than larger crystallites. Therefore the stability limit of PtO_x should change considerably (a_0^* should decrease) as crystallite size decreases. The present a_0^* values must correspond to the limit of large crystallites. Even with the catalyst film used a variety of crystallite sizes must exist so that the stability limit of platinum oxide could be more realistically represented by a band of a_0^* values rather than by a single value.

The key observation that leads to the proposed model is the electrochemically measured oxygen activity a_O. It would be interesting to examine if such a model could be used to describe other catalytic oscillatory reactions on platinum.

APPENDIX: NOTATION

Symbols

a_O = Oxygen activity, $bar^{1/2}$
c_1 = Oxygen concentration, $mole/cm^3$
c_2 = Ethylene concentration, $mole/cm^3$
c_T = Total gas concentration, $mole/cm^3$
C_m = Surface concentration of oxygen on m sites at full coverage, gram $atom/cm^2$
C_1 = Surface concentration of oxygen on 1 sites at full coverage, gram $atom/cm^2$
F = Volumetric flow rate, cm^3STP/s
F' = Faraday constant
k_1 = Specific rate constant for reaction (8a), $mole/cm^2 \cdot s$
k_2 = Specific rate constant for reaction (9), $mole/cm^2 \cdot s$
k_3 = Specific rate constant for reaction (10), $mole/cm^2 \cdot s$
k_4 = Specific rate constant for reaction (11), $mole/cm^2 \cdot s$
K_1 = Rate constant for reaction (8a), mole/s
K_2 = Rate constant for reaction (9), mole/s
$N_1 = S \cdot k_1/F \cdot c_T$
$N_2 = S \cdot k_2/F \cdot c_T$
$N_3 = c_{2f}/c_{1f}$, $N_4 = S \cdot k_4/F \cdot c_T$
$N_5 = S \cdot C_m/Vc_{1f}$
$N_6 = S \cdot C_1/Vc_{1f}$
$N_7 = S \cdot k_3/Fc_{1f}$
$P_{O_2} = c_1/c_T$
$P_{ET} = c_2/c_T$
R = 1.987 cal/mole · K
R_s = dimensionless rate of ethylene oxidation
S = catalyst surface area, cm^2
t_* = real time, s
t = dimensionless time, $t_* \cdot F/V$
T_p = period of limit cycle, s
V = reactor volume
$x_1 = c_1/c_{1f}$
$x_2 = c_2/c_{1f}$

Greek Letters

α = Heaviside function defined by (19)
γ = dimensionless constant
θ_1 = oxygen coverage on m sites, dimensionless
θ_2 = oxygen coverage on 1 sites, dimensionless
θ = reactor mean residence time, s
ν = limit cycle frequency, s^{-1}

Subscripts

f : reactor feed conditions
s : steady state

ACKNOWLEDGMENTS

This research was supported by the NSF under Grant ENG 77-27500. Acknowledgment is also made to the Donors of the PRF for partial support of this research under Grant 9893-G3.

REFERENCES

1. Margolis, L. Y., *Advan. Catal.* **14**, 429 (1963).
2. Voge, H. H., and Adams, C. R., *Advan. Catal.* **17**, 151 (1967).
3. Cant, N. W., and Hall, W. K., *J. Catal.* **16**, 220 (1970).
4. Carberry, J. J., *Kinet. Katal.* **18**(3), 562 (1977).
5. Hawkins, J. R., and Wanke, S. E., *in* "Proceedings, 5th Can. Symp. Catal., 1977," p. 245.
6. Wagner, C., *Advan. Catal.* **21**, 323 (1970).
7. Vayenas, C. G., and Saltsburg, H. M., *J. Catal.* **57**, 296 (1979).
8. Stoukides, M., and Vayenas, C. G., *J. Catal.* **64**, 18 (1980).
9. Vayenas, C. G., Lee, B., and Michaels, J., *J. Catal.* **66**, 36 (1980).
10. Scheintuch, M., and Schmitz, R. A., *Catal. Rev. Sci. Eng.* **15**, 107 (1977).

11. Schmitz, R. A., *Proc. JACC* **2,** 21 (1978).
12. Sheintuch, M., and Schmitz, R. A., *ACS Symp. Ser.* **165,** 487 (1978).
13. Pikios, C. A., and Luss, D., *Chem. Eng. Sci.* **32,** 191 (1977).
14. Eigenberger, G., *Chem. Eng. Sci.* **33,** 1263 (1978).
15. Boudart, M., Hanson, F. V., and Beegle, B., Paper presented at AIChE Meeting, Chicago, Ill. November 1976.
16. McCarthy, E., Zahradnik, J., Kuczynski, G. C., and Carberry, J. J., *J. Catal.* **39,** 29 (1975).
17. Varghese, P., Carberry, J. J., and Wolf, E. E., *J. Catal.* **55,** 76 (1978).
18. Kurtanjek, Z., Sheintuch, M., and Luss, D., *Ber. Bunsenges. Phys. Chem.* **84,** 374 (1980).
19. Dauchot, J. P., and Van Cakenberghe, J., *Nature (Phys. Sci.)* **246**(152), 61 (1973).
20. Dagonnier, R., and Nuyts, J., *J. Chem. Phys.* **65,** 2061 (1976).
21. Slinko, M. G., and Slinko, M. M., *Catal. Rev. Sci. Eng.* **17,** 119 (1978).
22. Hetrick, R. E., and Logothetis, E. M., *Appl. Phys. Lett.* **34**(1), 117 (1979).
23. Cutlip, M. B., and Kenney, C. N., *ACS Symp. Ser.* **165,** 475 (1978).
24. Ostermaier, J. J., Katzer, J. R., and Manogue, W. H., *J. Catal.* **41,** 277 (1976).
25. Gland, J. L., and Korchak, V. N., *Surface Sci.* **75,** 733 (1978).
26. Matsushima, T., Almy, D. B., and White, J. M., *Surface Sci.* **67,** 89 (1977).
27. Lee, B., M.S. thesis, Massachusetts Institute of Technology, 1979.